Journal of Materials Chemistry A



PAPER



Cite this: J. Mater. Chem. A, 2020, 8, 12457

Received 18th March 2020 Accepted 3rd June 2020

DOI: 10.1039/d0ta03099f

rsc.li/materials-a

Bimetallenes for selective electrocatalytic conversion of CO₂: a first-principles study†

Zhonglong Zhao (Dang Lu*b)

Two-dimensional (2D) materials are full of surprises and fascinating potential. Motivated by a recent discovery that sub-nanometer PdMo bimetallenes can realize exceptional performance in the oxygen reduction reaction [Nature 2019, 574, 81–85], we explore the potential of 2D bimetallenes for catalyzing the CO₂ electroreduction reaction (CO₂RR). Following extensive first-principles calculations on more than a hundred bimetallenes, we identify 17 Cu- and Ag-based bimetallenes, which are highly active and selective toward the formation of formic acid and simultaneously suppress the competing hydrogen evolution reaction. Equally important, we find that CO₂RR products *via* intermediates of COOH and CO are disfavored on these bimetallenes. Although surface strains are developed on the bimetallenes, their contribution to the catalytic activities is moderate as compared to that of the alloying effect. This work opens the door to future applications of bimetallenes as active and selective catalysts for the CO₂RR.

1. Introduction

With renewable solar, hydro, and wind energy as inputs, CO2 can be converted electrochemically into value-added chemicals and fuels, such as formic acid (HCOOH), carbon monoxide (CO), methane (CH₄), methanol (CH₃OH), ethylene (C_2H_4), etc. It is widely recognized that the electrochemical CO₂ reduction reaction (CO₂RR) is one of the most attractive means to mitigate pressing energy and environmental threats.1-3 Transition metals, such as Cu, Au, Ag, Pd, and Pt and their alloys are known to be active in catalyzing the CO₂RR.⁴⁻¹⁰ However, they suffer from sluggish kinetics and poor selectivity. For example, Cu is among the most active pure metal catalysts for the CO₂RR, capable of producing significant amounts of hydrocarbons, such as CH₄ and C₂H₄. However, a very high overpotential of \sim 1 V vs. reversible hydrogen electrode (RHE) is required for the reaction in which more than a dozen byproducts can be formed.^{7,11} In addition, the hydrogen evolution reaction (HER) is highly active on metal catalysts, consuming protons from the solvent, and thus competes with the CO₂RR.^{12,13} For example, the faradaic efficiency (FE) of the HER on Fe, Ni, and Pt is close to 90% at 1 V vs. RHE, while the FE of the CO₂RR is less than 4% on the same surfaces.8 Lastly, on some metals, such as Pd, CO poisoning can be problematic due to its strong binding to active sites.14-17 Therefore, it is of great scientific and technological interest to discover novel metal catalysts that can overcome the

aforementioned problems and are both active and selective towards the $\mathrm{CO}_2\mathrm{RR}$.

Recently, a new class of materials - two-dimensional (2D) metals - have shown tremendous promise to overcome these challenges. 18 Compared to bulk materials, 2D metals possess abundant active sites thanks to their extremely large surface-tovolume ratios, leading to exceptional catalytic activities. For example, Co and partially oxidized Co nanosheets with a thickness of \sim 0.84 nm (4-atom-thick) can produce formate with an ultrahigh FE of 90%, at a current density of 10 mA cm⁻² and a potential of 0.24 V vs. RHE.19 Similarly, hybrid Cu/Ni(OH)2 nanosheets can achieve a current density of 4.3 mA cm⁻² and a FE of 92% at 0.39 V vs. RHE for the CO₂RR to CO.20 Zn nanosheets coated with ZnS layers and Bi nanosheets are also found to be active for CO2 reduction to CO and formate, respectively, with an FE of more than 90% at ~0.8 V vs. RHE. 21-23 Recently, our work has shown that 4-atom-thick PdMo nanosheets can deliver a mass activity of 16.37 A mg_{Pd}⁻¹ for the oxygen reduction reaction (ORR), which is 327 times greater than that of the commercial Pd/C.24 These PdMo nanosheets are also quite stable, retaining much of their initial mass activity after 30 000 cycles. Importantly, different binary alloy nanosheets or "bimetallenes" can be synthesized by following the same protocols but with different reactants. For example, a PdMo bimetallene can be synthesized by heating a homogeneous solution of Pd(acac)2, Mo(CO)6, ascorbic acid, and oleylamine at 80 °C for 12 hours. By simply switching Mo(CO)₆ to W(CO)₆ or CO, PdW or pure Pd bimetallenes can be obtained.²⁴ Therefore, these bimetallenes are anticipated to be widely useful as electrocatalysts, and in this work, we explore their potential application in the CO₂RR.

[&]quot;School of Physical Science and Technology, Inner Mongolia University, Hohhot 010021, China

^bDepartment of Physics and Astronomy, California State University Northridge, California 91330, USA. E-mail: ganglu@csun.edu

[†] Electronic supplementary information (ESI) available. See DOI: 10.1039/d0ta03099f

Designing nanoscale alloys to improve catalytic activity and selectivity has been a successful strategy for electrocatalysis. 25,26 The electronic structure of a pure metal surface can be tuned by alloying, which in turn can modulate reaction pathways toward desired products. For example, we have shown that transition metal near-surface alloys can be engineered as highly selective CO₂RR catalysts toward specific products, such as HCOOH, CO, CH₄, and C₂H₄.²⁷ In this work, we will follow the same strategy and explore whether 2D bimetallenes can be designed as efficient catalysts for the CO2RR. To this end, we focus on five representative metal hosts (Cu, Ag, Au, Pd, and Pt) and combine them with 25 metal solutes (Ti, V, Cr, Mn, Fe, Co, Ni, Cu, Zn, Zr, Nb, Mo, Ru, Rh, Pd, Ag, Cd, Hf, Ta, W, Re, Os, Ir, Pt, Au) to form 120 distinct bimetallenes. We then assess the stability of these bimetallenes and select the stable ones for further study. Next, we calculate the reaction free energies of various reaction intermediates on these bimetallenes, from which we can identify promising bimetallenes for selective production of HCOOH. Finally, we examine the relative importance of strain, quantum size, and alloying effects on the CO2RR activities of the bimetallenes.

2. Computational details

The 2D bimetallenes are modeled by using a four-atomic-layer slab with a 4×4 in-plane supercell (64 atoms) and exposed (111) facets. As shown in Fig. 1, the solute atoms at a concentration of 12.5% are uniformly distributed in layer 2 and 3; this model has been used to represent the atomic arrangement in the PdMo bimetallene.²⁴ The equilibrium lattice parameter of Cu, Ag, Au, Pd, and Pt is determined to be 3.636, 4.162, 4.172, 3.952, and 3.976 Å, respectively. The adjacent slabs are separated by a 15 Å vacuum in the normal direction.

First-principles calculations are carried out using the Vienna $Ab\ initio$ Simulation Package (VASP)²⁸ with a revised Perdew–Burke–Ernzerhof (RPBE) functional^{29,30} and projector augmented wave pseudopotentials.³¹ The plane-wave energy cutoff is taken as 400 eV and the Brillouin-zone is sampled with a 3 \times 3 \times 1 k-mesh according to the Monkhorst–Pack scheme.³² All the atomic structures are optimized until the forces are less than 0.02 eV Å⁻¹. Spin-polarized calculations are performed for the bimetallenes with magnetic solutes (Cr, Mn, Fe, Co, and Ni).

Ultrathin 2D materials are usually thermodynamically less stable than bulk phases.³³ Therefore, instead of evaluating the

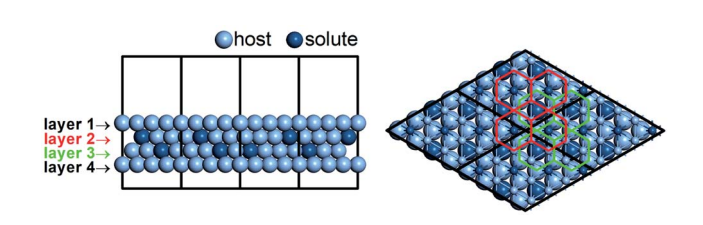


Fig. 1 Side view (left) and top view (right) of the slab model for the four-layer bimetallene, showing the atomic arrangement in layer 2 and 3. Each solute atom in layer 2 and 3 is surrounded by six host atoms, indicated by red and green hexagons, respectively.

formation energy of the bimetallenes, we calculate the segregation energy of each solute,34 which is defined as the energy required for a solute atom migrating from the interior (layer 2 or layer 3) to the surfaces (layer 1 or layer 4), i.e., $E_{\text{seg}} = E_{\text{surface}}$ (solute) – E_{interior} (solute). A positive segregation energy indicates that the migration is endothermic and the bimetallene is considered stable against the dissolution of the solute. In this way, 103 stable bimetallenes are identified (Table S1†) and will be the subject of the following study. Ab initio molecular dynamics (MD) simulations are subsequently performed to validate the stability of a subset of the bimetallenes. The proposed bimetallenes are found to be stable during the MD simulations, evidenced by negligible changes in the radial distribution functions (Fig. S1†). Since oxophilic Mo and W solutes retain their metallic states in synthesized PdMo and PdW bimetallenes,24 the oxidation of the solutes in the proposed bimetallenes is not studied. We should emphasize that precise control of preparation conditions is key to synthesizing the proposed bimetallenes.24

The computational hydrogen electrode (CHE) model is employed to estimate the free energy for each reaction step of the CO₂RR.³⁵ In the CHE model, the chemical potential of a proton-electron pair is defined in equilibrium with a half of the chemical potential of gaseous H₂ at 0 V, 101 325 Pa, and any pH values, i.e., $\mu(H^+ + e^-) = \mu(H_2)/2$. When an external potential U is applied to the catalyst, $\mu(H^+ + e^-)$ is shifted by -eU(e) is the elementary positive charge). Details about the free energy calculations can be found in the ESI.† The free energy barriers for various reactions are determined using the climbing-imagenudged elastic band (CI-NEB) method.36 The ab initio MD simulations are performed at 300 K using an NVT ensemble. 37-39 An 8×8 in-plane supercell (256 atoms) is used and the duration of each MD simulation is 4 ps (with a time step of 1 fs). Classical MD simulations are also performed at 300 K to determine the surface strains on selected bimetallenes using the LAMMPS package⁴⁰ with an NVT ensemble and EAM potentials.⁴¹ A 50 × 50 nm supercell with 149 760 atoms is adopted and 500 000 MD steps (with a time-step of 1 fs) are performed in each classical MD simulation.

Results and discussion

To design catalysts for the CO_2RR , one has to take into consideration the competing reaction, HER. There are two reaction steps in the HER: $^*+(H^++e^-) \rightarrow H^*$ and $H^*+(H^++e^-) \rightarrow H_2$; here * and H^* represent the clean surface and adsorbed H species, respectively. Since H^* is the only intermediate in the HER, it follows from the Sabatier principle that a moderate binding of H^* to the surface would result in a high HER activity, *i.e.*, near the "volcano" top. 42 A very strong or weak binding of H^* to the surface, on the other hand, would make the catalyst descend from the "volcano" top with increased HER overpotential. It is generally believed that the competition between the CO_2RR and the HER is determined by the relative stability of their respective first intermediates. 27 If the first intermediates of the CO_2RR (*i.e.*, $COOH^*$ or $HCOO^*)^{5,6,15,27}$ are more stable than

 H^* of the HER, they will occupy the active sites so that the CO_2RR would dominate. Conversely, the HER would prevail.

To assess the competition between the HER and the CO₂RR on the bimetallenes, we compare the formation free energy of $H^* (\Delta G[^* \to H^*])$ to that of COOH* or HCOO* $(\Delta G[CO_2 \to H^*])$ COOH*/HCOO*]) on the proposed bimetallenes, as shown in Fig. 2. The bimetallenes on the lower-right in Fig. 2 are predicted to have weak binding of H* to the surface and high overpotentials for the HER, and thus are considered as promising candidates for CO₂RR catalysts. It is found that most Au-, Pd-, and Pt-based bimetallenes are active for the initial step of CO2 reduction to COOH* (squares in Fig. 2), while Cu- and Agbased bimetallenes are active for CO2 reduction to HCOO* (circles in Fig. 2). In particular, five bimetallenes (CuZr, AgFe, AgCo, AgCu, and AgMn) are below the orange isoline in Fig. 2, indicating that the formation free energy of HCOO* is lower than that of H*. In other words, as far as the first step is concerned, these bimetallenes are more active for the CO₂RR than the HER. In addition, we include in our study the bimetallenes that have slightly higher formation energies towards the CO₂RR than the HER. We take $\Delta G[CO_2 \rightarrow COOH^*/HCOO^*]$ on Ag (111) as the reference (cyan isoline in Fig. 2) since bulk Ag is a decent CO2RR catalyst with a FE of HER about 10%.8 These bimetallenes (CuHf, CuCo, AgPt, AgOs, AgRe, AgW, AgTa, AgHf, AgPd, AgRu, AgNb, AgZr AgNi, AgCr, AgV, and AgTi) shown in the orange area of Fig. 2 are also considered as potential catalysts for the CO₂RR.

We next pay closer attention to these 21 promising bimetallenes. They are all found to be active in reducing CO_2 to $HCOO^*$ (Fig. 2). As summarized in Table S2,† the increases of free energy on these bimetallenes toward the formation of $HCOO^*$ are less than half of those toward the formation of $COOH^*$. Furthermore, $HCOO^*$ can be reduced to either H_2COO^* or $HCOOH^*$ with one proton transferred to a C or O

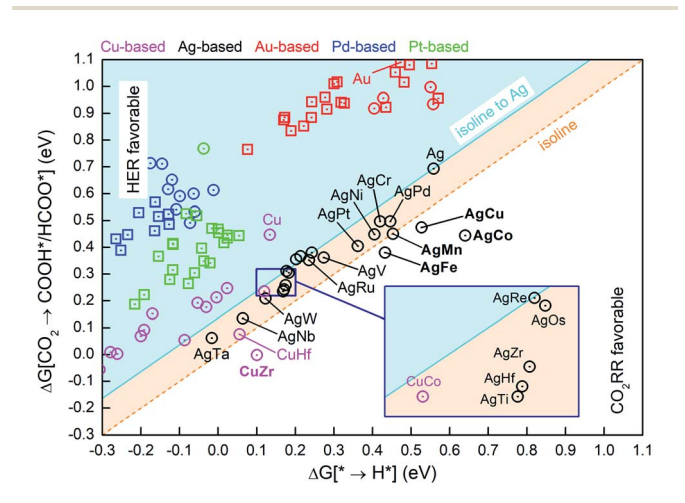


Fig. 2 Changes in the free energy for the formation of the favorable intermediate, COOH* (squares) or HCOO* (circles), in the initial step of the CO $_2$ RR against changes in the free energy for the formation of H* on the 103 proposed bimetallenes. Above the orange iso-energy line (isoline), the HER is more active, and below it, the CO $_2$ RR is more active. The cyan isoline refers to the changes in the intermediate free energy on Ag (111).

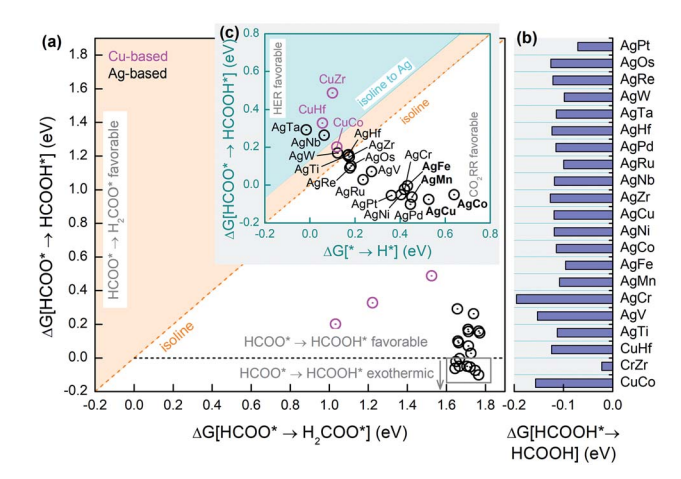


Fig. 3 (a) Changes in the free energy for the reduction of HCOO* to HCOOH* against changes in the free energy for the formation of H_2COO * on the 21 proposed bimetallenes. Below the orange isoline, HCOO* \rightarrow HCOOH* is more active. (b) Column chart of the changes in the free energy for the desorption of HCOOH* on the proposed bimetallenes. (c) Changes in the free energy for the reduction of HCOO* to HCOOH* against changes in the free energy for the formation of H* on the proposed bimetallenes. Above the orange isoline, the HER is more active, and below it, the CO2RR is more active. The cyan isoline refers to the changes in the intermediate free energy on Ag (111).

atom, respectively.5 Fig. 3a shows the changes of free energy reducing HCOO* to either H2COO* or HCOOH* on the 21 bimetallenes. It is found that the reduction of HCOO* to HCOOH* is favored over that to H2COO* on all 21 bimetallenes, and the reaction is even exothermic on Ag-based bimetallenes (AgCr, AgMn, AgFe, AgCo, AgNi, AgCu, AgPd, and AgPt). In addition, the desorption of HCOOH* from the bimetallene surfaces is also exothermic (Fig. 3b). Therefore, these bimetallenes are predicted to be selective catalysts for CO₂ reduction to HCOOH. As efficient HCOOH catalysts, the free energy change for the second hydrogenation step (HCOO* \rightarrow HCOOH) along the established reaction pathway $(CO_2 \rightarrow HCOO^* \rightarrow HCOO^*)$ $HCOOH^* \rightarrow HCOOH$) should be lower or comparable to ΔG [* \rightarrow H*]. As shown in Fig. 3c, 17 of the 21 bimetallenes are below the isoline, meeting this requirement. As one of the simplest products of the CO₂RR, HCOOH has applications in fuel cells, hydrogen storage, and chemical synthesis. 43-45

Fig. 4a, b, and S2† show the free energy diagrams for the formation of HCOOH and HER on the 17 proposed bimetallenes. It is revealed that the first reaction, *i.e.*, the reduction of CO₂ to HCOO* is the overpotential-determining step for the production of HCOOH. The HER is suppressed on AgMn, AgFe, AgCo, and AgCu bimetallenes since the free energy increase in the overpotential-determining step is lower than that for the HER, rendering the catalysts highly selective for the CO₂RR. Moreover, AgW, AgTi, AgHf, AgZr, and CuCo bimetallenes are predicted to be highly active HCOOH catalysts due to their low overpotentials calculated to be 0.21, 0.24, 0.24, 0.26, and 0.24 V vs. RHE, respectively. These values are comparable to those found in the most active HCOOH catalysts, such as partially oxidized Co nanosheets (0.24 V vs. RHE).¹⁹

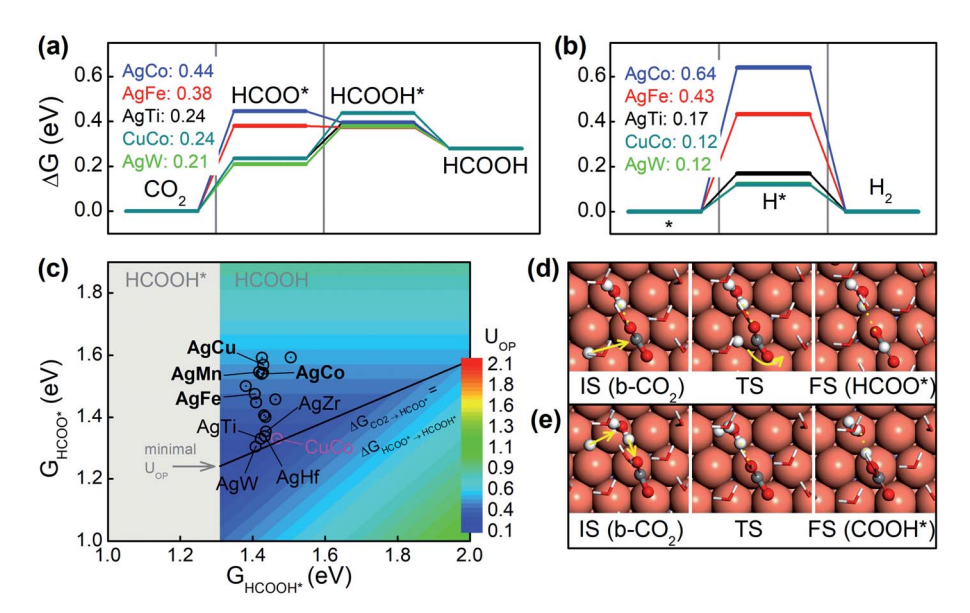


Fig. 4 Free energy diagrams toward HCOOH production (a) and the HER (b) on selected bimetallenes. (c) Overpotential contour map toward HCOOH production in terms of the free energies of HCOO* and HCOOH*. The optimized atomic geometries of the initial state (IS), transition state (TS), and final state (FS) for the hydrogenation of (d) b-CO₂ to HCOO* and (e) from b-CO₂ to COOH* on the CuCo bimetallene. Large orange, gray, red, and white spheres represent Cu, C, O, and H atoms, respectively.

To place the above results in a more general context, we consider the same reaction pathway for CO2 reduction to HCOOH on an arbitrary catalyst using the same computational model. We first note that the free energies of the initial state (CO₂) and the final state (HCOOH) are constant, independent of the catalyst. We also note that in a two-step reaction, each step has an overpotential and the overall overpotential of the reaction is the greater than the two. Hence, in a two-step reaction with a fixed free energy difference between the initial and final states, the overall overpotential is minimized when the overpotentials of the two separate steps are the same. Accordingly, we can define an overpotential "trough" (or a minimal overpotential line) on which $\Delta G_{\text{CO}_2 \to \text{HCOO}^*}$ equals $\Delta G_{\text{HCOO}^* \to}$ HCOOH*. The overpotential trough (the black line in Fig. 4c) represents the minimal overpotential of the reaction for a given value of G_{HCOOH} . Since it is energetically unfavorable for HCOOH* to desorb from the surface if $\Delta G_{\text{HCOOH*} \rightarrow \text{HCOOH}}$ < 0 (or G_{HCOOH^*} < 1.31 eV), the gray area in the figure is excluded from the overpotential trough. Interestingly, we find the predicted AgW, AgTi, AgHf, AgZr, and CuCo bimetallenes to be very close to the minimal overpotential line, suggesting that these bimetallenes are among the most active metal catalysts for CO₂ reduction to HCOOH.

Our study has established that the initial reduction of CO₂ to HCOO* (instead of COOH*) is a key step for the selective formation of HCOOH on the bimetallenes. Although it is long believed that CO₂ can only physisorb on Cu surfaces, a recent study has suggested that CO₂ can also chemisorb on Cu (100) and (111) surfaces as a bent radical anion (b-CO₂) under voltage. ⁴⁶ Since b-CO₂ is anchored on the metal surface *via* the C atom, the hydrogenation of b-CO₂ to form HCOO* may be hindered due to C-surface bonding. ^{47,48} Here we examine the

hydrogenation mechanism of b-CO₂ on bimetallenes, with CuCo as an example, by calculating the activation barriers. 49,50 Interestingly, we uncover a low-barrier (0.36 eV) reaction pathway for the hydrogenation of b-CO₂ toward HCOO*, which involves a proton transfer to the C atom and a simultaneous rotation of b-CO2 to form a C-H bond, shown schematically in Fig. 4d. The branched pathway (from b-CO₂ to COOH*), which takes place via a simultaneous proton transfer from the surface to a water molecule in the solvent and from the water molecule to the O atom in b-CO₂ (Fig. 4e), has a much higher barrier of 0.86 eV. Given this high barrier, a voltage of 0.93 V vs. RHE has to be applied to start the reduction (assuming the maximum barrier surmountable at room temperature is 0.4 eV). Therefore, the HCOO pathway is favored on the proposed bimetallenes owing to lower free energy and activation energy. Details about the reaction model and the activation energy calculations can be found in the ESI.†

Strain and quantum confinement (or size) effects could also play important roles in determining the catalytic activities of bimetallenes, in addition to chemical compositions.²⁴ To assess their contributions, we perform classical MD simulations to estimate the surface strains on the bimetallenes. We find that compressive strains are developed on bimetallenes when a smaller 3d solute is integrated in to a larger 4d host matrix. For example, the average surface compression on the AgFe bimetallene is calculated to be 0.71% due to the metallic radius difference between Ag (144 pm) and Fe (126 pm). However, the effect of surface strains on the reaction free energy is found to be moderate, owing to minor responses of the d-band center to the surface strains. For example, the free energy change for H* on AgFe is merely 0.01 eV under a 1% compressive strain. As shown in Fig. 5a and b, the shift in the

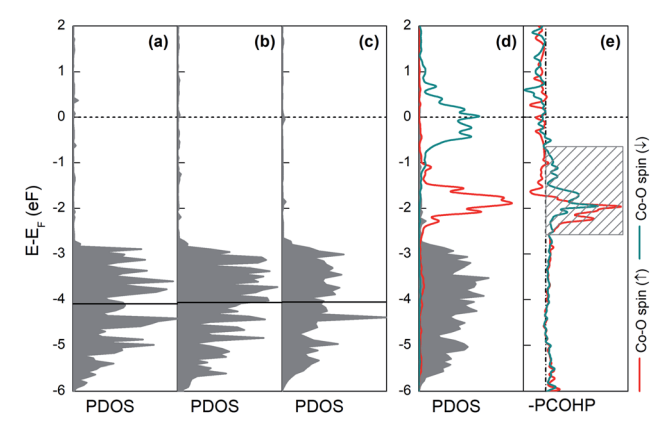


Fig. 5 Projected density of states (PDOS) for the d-band of the surface atoms (gray curves) in (a) Ag bimetallene, (b) Ag bimetallene under 1% compression, (c) bulk Ag, and (d) AgCo bimetallene. The d-band of the sublayer Co atoms in the AgCo bimetallene is shown as red (spin up) and cyan (spin down) curves in (d). The horizontal dashed and solid lines indicate the Fermi level and the d-band centers, respectively. (e) The projected crystal orbital Hamilton population (PCOHP) for the Co–O bonds in the HCOO-adsorbed AgCo bimetallene. Bonding and antibonding states are shown on the right and left, respectively. The bonding states between the sublayer Co and surface HCOO* below the Fermi level (–0.6 to –2.6 eV) are highlighted by a shadow area.

d-band center of the surface Ag atoms on a pure Ag bimetallene is only 29 meV under a 1% compression. Similarly, the quantum confinement effect is found to be small too. As shown in Fig. 5a and c, the shift in the d-band center of the surface atoms on the Ag bimetallene, relative to the d-band center on bulk Ag is merely ~40 meV. By contrast, chemical composition or alloying has a much greater effect on the dband structure of bimetallenes. For example, alloying Co with the Ag bimetallene drastically modifies the density of states (DOS) near the Fermi energy (Fig. 5d), and the newly formed states interact strongly with the reaction intermediates. More specifically, when HCOO* is adsorbed on the AgCo bimetallene, bonding states between the sublayer Co and the O atom of the adsorbed HCOO* emerge at -0.6 to -2.6 eV, according to the projected crystal orbital Hamilton population (PCOHP)51,52 analysis shown in Fig. 5e. The fact that the chemical composition plays a more important role than the strain and quantum confinement was also observed in the oxygen reduction reaction on the bimetallenes.24 Although the strain and quantum confinement are less effective in changing the reaction energies, they are nonetheless useful means to tune the catalytic performance, in addition to alloying. We have shown that surface compressions can be developed on the AgFe bimetallene by integrating smaller Fe solutes into the Ag host. Conversely, we can also generate surface tensions by incorporating larger solutes into the host. For example, we can create an average surface tension of 1.23% on the CuW bimetallene. Even though the quantum size effect may not be so important, ultrathin bimetallenes could yield large surface areas and lead to exceedingly high mass activities.24 Finally, it is of interest to examine whether bimetallenes can bring more surprises in other complex chemical reactions, such as ammonia synthesis.

4. Conclusions

In summary, we have systematically examined a new class of nano-metals, bimetallenes, as catalysts for the CO2RR from first-principles calculations. We have identified 21 Cu- and Agbased bimetallenes which are more active toward the formation of HCOO* in the first hydrogenation step of the CO₂RR. Among them, 17 bimetallenes (CuCo, AgTi, AgV, AgCr, AgMn, AgFe, AgCo, AgNi, AgCu, AgZr, AgRu, AgPd, AgHf, AgW, AgRe, AgOs, and AgPt) are found to be highly selective toward the formation of HCOOH as the final product. Five of the identified bimetallenes (CuCo, AgTi, AgZr, AgHf, and AgW) are predicted to have overpotentials comparable to those of some of the most active electrocatalysts for the CO2RR. In addition, the HER is predicted to be completely suppressed on four of these 2D catalysts (AgMn, AgFe, AgCo, and AgCu). The reaction barrier for the hydrogenation of CO2 to HCOO* is found to be much lower than that for the reduction of CO2 to COOH*, which deactivates the formation of COOH* and CO*. Finally, we attribute the catalytic activity of the bimetallenes primarily to the alloying effect. This work provides crucial insights into the design of 2D metal nanocatalysts for the CO₂RR.

Conflicts of interest

There are no conflicts to declare.

Acknowledgements

Z. Z. was supported by a startup grant from Inner Mongolia University (21200-5195113) in China and G. L. was supported by the PREM program (DMR-1828019) from the US National Science Foundation.

References

- 1 N. S. Lewis and D. G. Nocera, *Proc. Natl. Acad. Sci. U.S.A.*, 2006, **103**, 15729–15735.
- 2 G. A. Olah, G. K. S. Prakash and A. Goeppert, *J. Am. Chem. Soc.*, 2011, 133, 12881–12898.
- 3 H.-R. M. Jhong, S. Ma and P. J. A. Kenis, *Curr. Opin. Chem. Eng.*, 2013, **2**, 191–199.
- 4 Y. Hori, H. Wakebe, T. Tsukamoto and O. Koga, *Electrochim. Acta*, 1994, **39**, 1833–1839.
- 5 A. A. Peterson, F. Abild-Pedersen, F. Studt, J. Rossmeisl and J. K. Nørskov, *Energy Environ. Sci.*, 2010, 3, 1311–1315.
- 6 A. A. Peterson and J. K. Nørskov, *J. Phys. Chem. Lett.*, 2012, 3, 251–258.
- 7 K. P. Kuhl, E. R. Cave, D. N. Abram and T. F. Jaramillo, *Energy Environ. Sci.*, 2012, 5, 7050–7059.
- 8 K. P. Kuhl, T. Hatsukade, E. R. Cave, D. N. Abram, J. Kibsgaard and T. F. Jaramillo, *J. Am. Chem. Soc.*, 2014, **136**, 14107–14113.
- 9 Y. Li and Q. Sun, Adv. Energy Mater., 2016, 6, 1600463.
- 10 J. Qiao, Y. Liu, F. Hong and J. Zhang, Chem. Soc. Rev., 2014, 43, 631–675.

- 11 Y. Hori, A. Murata and R. Takahashi, *J. Chem. Soc., Perkin Trans.* 1, 1989, **85**, 2309–2326.
- 12 Y.-J. Zhang, V. Sethuraman, R. Michalsky and A. A. Peterson, *ACS Catal.*, 2014, 4, 3742–3748.
- 13 N. Elgrishi, M. B. Chambers and M. Fontecave, *Chem. Sci.*, 2015, **6**, 2522–2531.
- 14 S. A. Akhade, W. Luo, X. Nie, N. J. Bernstein, A. Asthagiri and M. J. Janik, *Phys. Chem. Chem. Phys.*, 2014, **16**, 20429–20435.
- 15 Z. Zhao, Z. Chen and G. Lu, J. Phys. Chem. C, 2017, 121, 20865–20870.
- 16 X. Min and M. W. Kanan, *J. Am. Chem. Soc.*, 2015, **137**, 4701–4708
- 17 A. Klinkova, P. De Luna, C.-T. Dinh, O. Voznyy, E. M. Larin, E. Kumacheva and E. H. Sargent, *ACS Catal.*, 2016, **6**, 8115–8120.
- 18 Y. Chen, Z. Fan, Z. Zhang, W. Niu, C. Li, N. Yang, B. Chen and H. Zhang, *Chem. Rev.*, 2018, **118**, 6409–6455.
- 19 S. Gao, Y. Lin, X. Jiao, Y. Sun, Q. Luo, W. Zhang, D. Li, J. Yang and Y. Xie, *Nature*, 2016, **529**, 68–71.
- 20 L. Dai, Q. Qin, P. Wang, X. Zhao, C. Hu, P. Liu, R. Qin, M. Chen, D. Ou, C. Xu, S. Mo, B. Wu, G. Fu, P. Zhang and N. Zheng, *Sci. Adv.*, 2017, 3, e1701069.
- 21 C. Li, G. Shen, R. Zhang, D. Wu, C. Zou, T. Ling, H. Liu, C. Dong and X.-W. Du, *J. Mater. Chem. A*, 2019, 7, 1418–1423.
- 22 W. Zhang, Y. Hu, L. Ma, G. Zhu, P. Zhao, X. Xue, R. Chen, S. Yang, J. Ma, J. Liu and Z. Jin, *Nano Energy*, 2018, 53, 808–816.
- 23 S.-X. Guo, Y. Zhang, X. Zhang, C. D. Easton, D. R. MacFarlane and J. Zhang, *ChemSusChem*, 2019, 12, 1091–1100.
- 24 M. Luo, Z. Zhao, Y. Zhang, Y. Sun, Y. Xing, F. Lv, Y. Yang, X. Zhang, S. Hwang, Y. Qin, J.-Y. Ma, F. Lin, D. Su, G. Lu and S. Guo, *Nature*, 2019, 574, 81–85.
- 25 C. Kim, F. Dionigi, V. Beermann, X. Wang, T. Möller and P. Strasser, *Adv. Mater.*, 2019, 31, 1805617.
- 26 J. W. Vickers, D. Alfonso and D. R. Kauffman, *Energy Technol.*, 2017, 5, 775–795.
- 27 Z. Zhao and G. Lu, ACS Catal., 2018, 8, 3885-3894.
- 28 G. Kresse and J. Furthmüller, *Phys. Rev. B*, 1996, **54**, 11169–11186
- 29 B. Hammer, L. B. Hansen and J. K. Nørskov, *Phys. Rev. B*, 1999, **59**, 7413–7421.

- 30 J. P. Perdew, K. Burke and M. Ernzerhof, *Phys. Rev. Lett.*, 1996, 77, 3865–3868.
- 31 P. E. Blöchl, Phys. Rev. B, 1994, 50, 17953-17979.
- 32 H. J. Monkhorst and J. D. Pack, *Phys. Rev. B*, 1976, **13**, 5188–5192.
- 33 K. D. Gilroy, A. Ruditskiy, H.-C. Peng, D. Qin and Y. Xia, *Chem. Rev.*, 2016, **116**, 10414–10472.
- 34 J. Greeley and M. Mavrikakis, Nat. Mater., 2004, 3, 810-815.
- 35 J. K. Nørskov, J. Rossmeisl, A. Logadottir, L. Lindqvist, J. R. Kitchin, T. Bligaard and H. Jónsson, *J. Phys. Chem. B*, 2004, **108**, 17886–17892.
- 36 G. Henkelman and H. Jónsson, *J. Chem. Phys.*, 2000, **113**, 9978–9985.
- 37 S. Nosé, J. Chem. Phys., 1984, 81, 511-519.
- 38 N. Shuichi, Prog. Theor. Phys. Suppl., 1991, 103, 1-46.
- 39 D. M. Bylander and L. Kleinman, *Phys. Rev. B*, 1992, **46**, 13756–13761.
- 40 S. Plimpton, J. Comput. Phys., 1995, 117, 1-19.
- 41 X. W. Zhou, R. A. Johnson and H. N. G. Wadley, *Phys. Rev. B*, 2004, **69**, 144113.
- 42 K. Chan, C. Tsai, H. A. Hansen and J. K. Nørskov, *ChemCatChem*, 2014, **6**, 1899–1905.
- 43 X. Yu and P. G. Pickup, *J. Power Sources*, 2008, **182**, 124–132.
- 44 M. G. Mura, L. D. Luca, G. Giacomelli and A. Porcheddu, *Adv. Synth. Catal.*, 2012, **354**, 3180–3186.
- 45 M. Grasemann and G. Laurenczy, *Energy Environ. Sci.*, 2012, 5, 8171–8181.
- 46 A. J. Garza, A. T. Bell and M. Head-Gordon, *J. Phys. Chem. Lett.*, 2018, **9**, 601–606.
- 47 H. He, P. Zapol and L. A. Curtiss, *Energy Environ. Sci.*, 2012, 5, 6196–6205.
- 48 Z. Zhao and G. Lu, J. Phys. Chem. C, 2019, 123, 4380-4387.
- 49 X. Nie, M. R. Esopi, M. J. Janik and A. Asthagiri, *Angew. Chem., Int. Ed.*, 2013, **52**, 2459–2462.
- 50 X. Nie, W. Luo, M. J. Janik and A. Asthagiri, *J. Catal.*, 2014, **312**, 108–122.
- 51 V. L. Deringer, A. L. Tchougréeff and R. Dronskowski, *J. Phys. Chem. A*, 2011, **115**, 5461–5466.
- 52 S. Maintz, V. L. Deringer, A. L. Tchougréeff and R. Dronskowski, *J. Comput. Chem.*, 2016, 37, 1030–1035.